Bio MACROMOLECULES

Article

Human Dermal Fibroblast Viability and Adhesion on Cellulose Nanomaterial Coatings: Influence of Surface Characteristics

Ruut Kummala, Diosángeles Soto Véliz, Zhiqiang Fang, Wenyang Xu, Tiffany Abitbol, Chunlin Xu, and Martti Toivakka*

Cite This: Biomacromolecules 2020, 21, 1560−1567

Read Online

ACCESS | Metrics & More | Article Recommendations | Supporting Information

ABSTRACT: Biodegradable and renewable materials, such as cellulose nanomaterials, have been studied as a replacement material for traditional plastics in the biomedical field. Furthermore, in chronic wound care, modern wound dressings, hydrogels, and active synthetic extracellular matrices promoting tissue regeneration are developed to guide cell growth and differentiation. Cells are guided not only by chemical cues but also through their interaction with the surrounding substrate and its physicochemical properties. Hence, the current work investigated plant-based cellulose nanomaterials and their surface characteristic effects on human dermal fibroblast (HDF) behavior. Four thin cellulose nanomaterial-based coatings produced from microfibrillar cellulose (MFC), cellulose nanocrystals (CNC), and two TEMPO-oxidized cellulose nanofibers (CNF) with different total surface charge were characterized, and HDF viability and adhesion were evaluated. The highest viability and most stable adhesion were on the anionic CNF coating with a surface charge of 1.14 mmol/g. On MFC and CNC coated surfaces, HDFs sedimented but were unable to anchor to the substrate, leading to low viability.
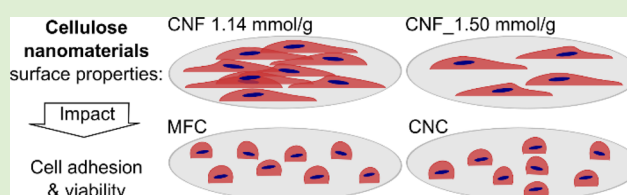
INTRODUCTION

Interest in green, renewable, and biodegradable materials has increased due to their potential as drug carriers, 3D cell cultures, wound dressings, and medical implants.[1] Bio-based nanofibrils, including cellulose, collagen, chitin, and silk, are of particular interest due to their suitable properties and adjustable mechanical properties of the larger structures made of them, satisfying biocompatibility[2] and low-cost.[3] The main applications for biopolymers in modern wound dressings are hydrogels that keep the wound moist, absorb wound exudate, behave as a barrier against bacteria, and permeate oxygen. These hydrogel dressings are replaced and removed after the wound is healed. Hence, adhesion and growth of cells into the hydrogel are not desired. But other more complex applications based on tissue engineering require cell growth, and active interactions with the extracellular matrix are expected.[4]

Cellulose nanomaterials (CNs) are fibers with at least one dimension at the nanoscale. Source material and isolation approach influence CN characteristics, such as its size, crystallinity, strength and surface chemistry. The fiber properties also control the properties of gel-like suspensions and dry films that can be produced from the fibers. CNs are categorized into bacterial nanocellulose (BNC), cellulose nanofibrils (CNFs), and cellulose nanocrystals (CNCs). BNC is synthesized extracellularly by bacteria, such as *Acetobacter xylinum*, from sugar units. CNCs and CNFs are usually isolated from plants, such as wood, using various combinations of mechanical, chemical, and enzymatic treat-ments.[5] CNFs are long nanofibrils consisting of both crystalline and less crystalline phases having a width of 5−60 nm and length in the range of 100 nm to several micrometers, and CNCs are rigid, rodlike nanoparticles having a width of 5−10 nm and length of 100−300 nm and are composed almost entirely of crystalline cellulose.[6]

BNC was the first type of CNs tested for biomedical applications due to its endotoxin- and residue-free nature. In biomedical applications, BNC has shown its potential, and various BNC-based wound healing products including Epiprotect and Celmat have been brought on the market.[4] Research on CN-based products focuses on wound healing substrates,[4,7−10] scaffolds for tissue engineering,[11−15] 3D cell culture systems, and controlled drug delivery.[16,17] An advantage of plant-based CNs is the possibility for large scale production to enable the development of low-cost products suitable for various biomedical end-uses.[17] For plant-based CNs, processing conditions are designed to produce materials free of bacterial endotoxins, which is a prerequisite for biomedical applications.[18] Furthermore, promising results from plant-based nanocellulose wound dressing has been reported.[8]

CNs have been studied for biomedical applications in different forms: as a hydrogel matrix, an aerogel, a film or as fibrils. As a single nanoparticle, CNCs can penetrate through the cell membrane without killing the cell due to their small width (5−15 nm) and rigid structure.[19,20] Thus, they are commonly studied as drug nanocarriers or as bioimaging probes. In nanocarrier and probe design, the surface chemistry and charge of the CNCs are essential factors affecting cell cytotoxicity and cellular uptake efficiency.[21−23] As films, CNs have been studied to understand the cell response to morphology and surface chemistry, characteristics known to be vital in defining the cells' ability to attach and differentiate.[24] For example, myoblasts cells can be aligned on a sub-monolayer of CNCs with a mean roughness of 5−6 nm.[25] Similar cell orientation was achieved on films of aligned cationically functionalized CNFs, and some alignment was observed on partially aligned anionic CNFs. Thin layers of collagen and fibronectin on BNC, CNCs, and CNFs have shown in some cases improvement of the adherence of the cells,[26−28] but especially uncharged grades produced mechanically show poor cell adhesion and reduced viability. Therefore, depending on the cell type, e.g., a fibroblast or a stem cell, and CN surface chemistry and morphology, differences in cell adhesion and viability can be expected. The CN gels have been studied for wound dressings and 3D cell culture platforms.[10,29,30] CN gelation is a prerequisite in adapting matrix stiffness to mimic the targeted tissue to improve biological responses of cells.[31] A thin layer of CNs forming a hydrogel in contact with water can be used to adjust the mechanical environment for cells, but it should be noted that with gel thickness below 10−20 μm cell growth can be affected by the underlying stiffer matrix.[32] The gel properties of CNs depend on fibril entanglement and surface charges, and properties of the liquid environment, type, and concentration of ions in the liquid phase.[7,33−35] CNs include a wide variety of fibers with size, crystallinity, and functional groups dependent on their origin, processing methods, and chemical functionalization. CN matrices and films are shown to support different degrees of cell viability.[1] However, the relationship between different cell behavior and characteristics of CNs remains unclear.

This study aims to show the effect of CN production methods on the properties of the as-prepared CN suspensions and coatings prepared from them. Furthermore, to clarify quantitatively human dermal fibroblast (HDF) adhesion and viability on CN coatings and their dependence on CN chemistry, morphology, and elasticity. Mechanically treated microfibrillar cellulose (MFC), two CNFs from TEMPO-mediated oxidation, and CNCs from sulfuric acid hydrolysis were produced and characterized. This is the first comparative study where HDF adhesion is quantitatively studied through focal adhesion sites to understand HDF behavior and viability on thin coatings made of common plant-based cellulose nanomaterials (CNC, CNF, and MFC).

■ EXPERIMENTAL SECTION

Four CNs were produced as detailed in Supporting Information Table S1. First, microfibrillated cellulose (MFC) from bleached softwood Kraft pulp was mechanically disintegrated using refiner with specialized plates at the University of Maine.[36] Two cellulose nanofibers (CNFs) were prepared by TEMPO-mediated oxidation and high-pressure homogenization. CNFs with low surface charge (CNF_L) were made at the Åbo Akademi University, and the CNFs with higher surface charge (CNF_M) were made at the South China University of Technology. The fourth CN was produced by sulfuric

acid hydrolysis to form cellulose nanocrystals (CNCs) at the Research Institutes of Sweden (RISE). Produced CNFs were transparent gel-like materials having a solids content of 0.4% and 0.9%. MFC was whiter and more solid-like gel at 2%, which was diluted to 1% before coating to improve its coatability. The last material CNC was a liquid suspension with a solids content of 1.3%.

Cellulose Nanomaterial Characterization. The size of the CNs was assessed from transmission electron microscopy (TEM, JEM-1400Plus, JEOL USA Inc.) images. A drop of 10 μL of a 0.01% CN suspension was placed on plasma-activated microscope grids, and excess water was removed using filter paper. Then, a drop of 2% uranyl acetate negative stain was used to stain the edges of the fibrils, and the excess was removed. One grid per sample type was imaged. The dried grids were imaged, and ImageJ[37] (version 1.51j8) software was used to measure dimensions of the fibrils in TEM images.

The total charge of TEMPO-treated CN grades was measured by conductometric titration from three replicates. First, in the 50 mL 0.1% CN suspension, 1.0 mL of 50 mM NaCl was added to improve conductivity together with 2 mL of 0.1 M HCl to protonate the surface charge groups. In the titration, 0.1 M NaOH was added at a rate of 0.1 mL/min while the conductivity and pH were measured. The total charge (σ) was calculated from recorded conductivity values as follows:

$$\sigma = \frac{c\Delta V}{m}$$

where c is the NaOH concentration (mol/L), m is the mass of dry CN (g), and ΔV is the difference between the volumes of NaOH needed to neutralize the weak acids and the strong acids.

The surface charge from the sulfuric acid groups ($-OSO_3^-$) on the CNCs was determined similarly from three replicates: 2 mL of 26 mM NaCl solution was added to 50 mL of 0.1% CNC solution to increase conductivity. Then, 2.2 mM NaOH was added at a rate of 0.15 mL/min. Here, only one equivalent point is obtained, which can be directly related to the strong acid sulfate half-ester content.

Cellulose Nanomaterial Coatings. CN suspensions were coated on latex-coated transparent polyester films (Melinex OD, 125 μm thick) by rod and blade coating methods. First, a thin layer of latex dispersion (styrene−butadiene copolymer, HPC26 experimental latex from Styron) solution (solids content of 50%) was coated with a rod having 24 μm theoretical wet film thickness to provide an adhesion layer for the CNs. The latex was cured at 80 °C for 5 min. The latex-coated plastic was washed with ethanol and deionized water prior to CN coating to remove possible leachable latex components. Three CN suspensions, MFC, CNF_L, and CNF_M, were coated with a blade coater having a theoretical dry film thickness of 24, 4, and 25 μm, respectively. Ethanol (5 v/v %) was mixed into the CNC suspension before coating to lower the surface tension enabling a full coating coverage with a 1 μm theoretical dry film thickness. All the CN coatings were dried at 80 °C.

On the thinnest coatings, CNC and CNF_L, some cracks formed during the drying process due to the stiffness of the thoroughly dried CNs on flexible plastic. On the thicker MFC and CNF_M coatings, dried films curled due to coating shrinkage. However, as the aim of the study was not to optimize the CN coating further, but instead to study cell adhesion and viability on CN coatings fully covering coatings without additives, these small defects were allowed.

A modification from a flexible cell culture plate setup developed by Soto Veliz et al.[38] was used to study cell adhesion and viability on CN coatings (Figure 1). Hydrophobic boundaries were printed onto the CN coated plastics using a wax printer (ColorQube 8580, Xerox) with black wax. The boundaries created circular wells of 10 mm in diameter. The patterned samples were cut from plastic sheets using a desktop precision cutter (Silver Bullet, Thyme Graphics). The hydrophobic wax patterns needed to be reinforced because they broke when the CN films swelled upon contact with the cell culture media. Hence, a layer of transparent polydimethylsiloxane (PDMS, Dehesive 915, Cross-linker V24, Catalyst OL, Wacker Chemie AG) was spray-coated around the wells and cured at 90 °C for 15 min.
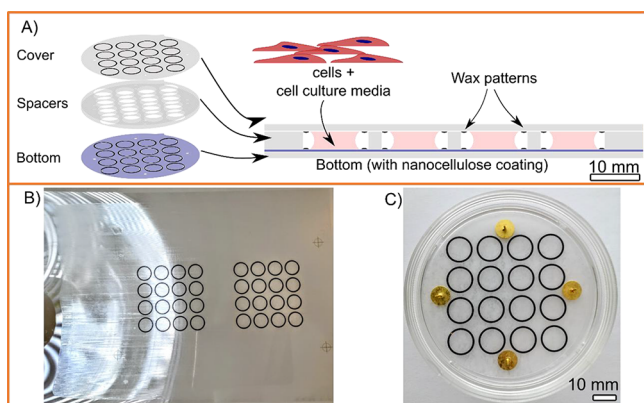
Figure 1. Schematic illustration showing (A) a sandwich test setup composed of a CN-coated bottom film, plastic spacers, and cover used to reduce the evaporation of cell culture media during cell studies, (B) the CN coated A4 sized sheets patterned with a wax printer before cutting, and (C) a finalized sample set in a dish with metal pins used to align the spacers and the cover.

Coating Characterization. Wetting properties of the coatings were studied using static contact angle measurements (KSV CAM 200, KSV Instruments Ltd., Finland). A 4 μL drop of purified water (Milli-Q filtration unit, Millipore, USA) was dispensed onto the dry CN coatings at room temperature. An average of three measurements, at 0.1 and 5 s, was used to quantify the change in the contact angle with time. The acquired images were analyzed using OneAttension software (Version 3.2, Biolin Scientific) with a circular fit.

Appropriate optical properties of cell culture substrates are essential if the cells are to be imaged through the films. Hence, total transmittance and haze were measured using a Lambda 900 UV/vis/NIR spectrophotometer (PerkinElmer) with an integrating sphere. Total transmission is the amount of light that passes through the film, whereas haze is the amount of light that undergoes wide-angle scattering, i.e., at angles larger than 2.5° from the normal. The measurement wavelength range was 250−800 nm with a step size of 2 nm. Two replicates were made of each measurement. The results are presented in the visible light region 400−700 nm. Total luminous transmittance and haze were calculated according to ASTM standard D1003. Films were studied as swollen in cell culture media, Dulbecco's modified Eagle's medium (DMEM, D6171, Sigma-Aldrich).

The CN coatings swell to form a hydrogel when immersed in fluids, which changes their mechanical properties. To quantify this, the elastic modulus of the gelled coatings was measured by atomic force microscopy from three areas (10 × 10 indentations per area) per sample (AFM; Zeiss LSM510 laser scanning confocal microscope with JPK Nanowizard II with liquid cell) using a colloidal probe (silicon dioxide sphere diameter 6.62 μm, sQube). Before measurement, the CN coatings were submerged in an excess of DMEM, phosphate buffer solution (PBS, L0615, Biowest), or purified water (18.2 MΩ cm, Milli-Q Integral ultrapure water, Type 1) overnight at 37 °C. Measurements were analyzed using JPK Data Processing software by fitting the acquired force curves with the Hertzian model. The built-in calibration feature of JPK AFM was used to measure the sensitivity and spring constants of the cantilevers.

Cell Studies. HDFs (human, neonatal, ATCC PCS-201-010) were chosen because of their role in wound healing and extensive usage as a model system in skin biology studies.[39,40] HDFs were cultivated in DMEM supplemented with 10% fetal bovine serum (FBS, Biowest), penicillin−streptomycin (10,000 units/10 mg per mL, Sigma-Aldrich), and L-glutamine (200 mM, Biowest). Cells were incubated at 37 °C with an atmosphere containing 5% CO_2 and 95% relative humidity. Subculture was done at 80−90% confluency (percentage of area covered by the cells).

Samples were sterilized with UV−C irradiation for 30 min. The planar wells were prewet with DMEM, followed by four cell seeding densities (one per row): 0, 6000, 13,000, and 19,000 cells/cm^2, to study fibroblast adhesion and viability. Viable cells in each well were stained with 5 μM Calcein-AM (ThermoFisher Scientific), a cell-permeant dye. Latex (LTX) was used as the reference coating since it serves as the binding layer for the CN coatings, and it has previously been shown to support cell growth.[41] Fluorescence images were acquired with a gel scanner iBright FL1000 imaging system (Thermo Fischer Scientific) with 488 nm excitation. The acquired tiff-images were analyzed using Image Lab 6.0.1 (Bio-Rad Laboratories, Inc.) to calculate average fluorescence. The reference row in each sample (0 cells/well) was used to define the background fluorescence. Three replicates for each coating type (LTX, MFC, CNF_L, CNF_M, CNCs) and two incubation times (24 h, 72 h) were used to calculate a mean fluorescence intensity to indicate the average cell viability on each coating and the respective standard deviation of the measurements. After scanning the plates, select wells were imaged using fluorescence microscopy (Axio Vert. A1, Carl Zeiss Microscopy, 10× objective) to observe cell morphology and distribution.

Immunofluorescence Staining for Cell Adhesion Studies. Cells were stained after 1 day of cell culture on the samples to observe cell adhesion. Briefly, samples were washed with PBS, fixated with 4% PFA (15 min), and washed three times with PBS (5 min/wash). Blocking and permeabilization were done with 10% FBS and 0.3% Triton X-100 in PBS (30 min). Then, the samples were incubated with a primary staining solution at 4 °C, including 10% FBS, 1:2000 anti-Vimentin (BioLegend), and 1:70 anti-Vinculin (abCam) in PBS (overnight). The secondary staining solution included 10% FBS, 1:2000 anti-chicken (ThermoFisher Scientific), 1:70 anti-rabbit (ThermoFisher Scientific), and 1:300 Alexa Fluor 633 phalloidin (ThermoFisher Scientific) in PBS (1 h). The staining was followed by incubation with 300 nM DAPI (ThermoFisher Scientific) to stain the nuclei and two washes with PBS (5 min/wash). Finally, samples were glued onto a microscope slide, with the cells facing outward. Then, coverslips were mounted on top of the cells with Mowiol+DABCO (Sigma-Aldrich). Images were collected with a spinning disk microscope through the coverslips mounted on top of the cells. Image processing was done with FijiImageJ[42,43] and CellProfiler.[44] Additional information for the immunofluorescence staining and the image processing is included in the Supporting Information.

RESULTS AND DISCUSSION

CNs were prepared from bleached dried pulps and cotton using a combination of mechanical and chemical treatments. Depending on the method, different fibril sizes and surface charges are obtained. Fibril characteristics are summarized in the Supporting Information Table S2. MFC, which was produced solely through mechanical treatment, has a low surface charge and the largest fibrils, bundled together when compared to the three chemically pretreated CNs, as shown in Figure 2. The total charge of the MFC was 0.12 mmol/g, which is equal to the total charge of the bleached pulp before mechanical treatment. In TEMPO-mediated oxidation, C-6 hydroxyl groups of cellulose are replaced by negatively charged carboxyl groups increasing the surface charge of the fibrils. The TEMPO-treated CNFs labeled CNF_L and CNF_M had surface charges of 1.14 mmol/g and 1.50 mmol/g, respectively. TEMPO-treatment, along with high-pressure homogenization, led to long and thin individualized nanofibrils as shown in the TEM images (Figure 2). The higher oxidation level reduced the length of the fibrils, decreasing the aspect ratio from ca. 173 to 75 for CNF_M. The CNCs, prepared by sulfuric acid hydrolysis, show the typical rod-shaped morphology and a surface charge density of 0.25 mmol/g originating from the sulfate half-ester groups grafted onto the CNC surfaces during hydrolysis.[16]

Optical Characterization of the Cellulose Nanomaterial Coatings. Figure 3 shows total luminous transmittance
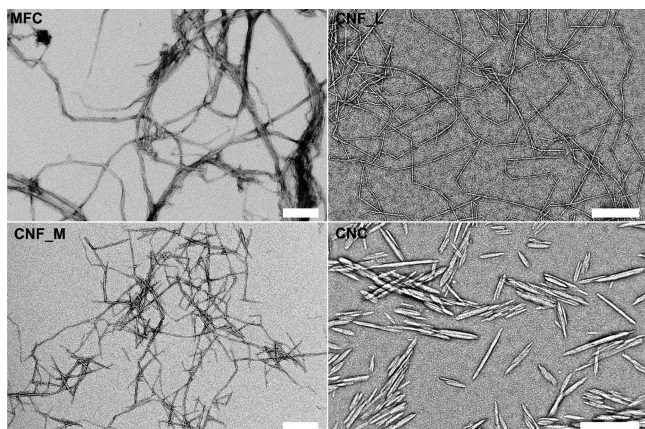
Figure 2. Size and shape of the fibrils MFC, CNF_L, CNF_M, and CNCs (scale bar: 200 nm).
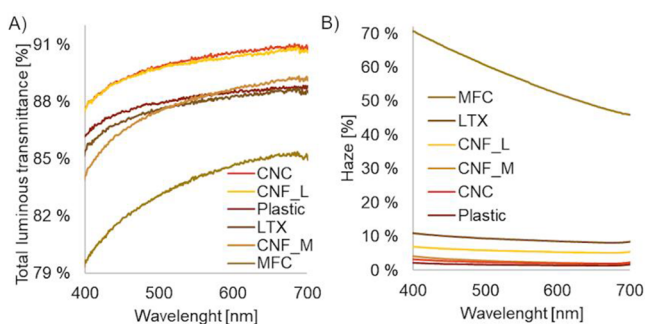

Figure 3. Total luminous transmittance (T) [%] (A) and transmittance haze (H) [%] (B) of the uncoated and coated films after wetting with DMEM. Sample headings are in same order as the lines the graphs.

and haze for the support plastic, the latex coated plastic, and the CN coatings after immersion in cell culture media for 6 h. Total luminous transmittance varied between 79 and 90% and haze between 1 and 71% across the visible light region (wavelength range 400−700 nm), as shown in Figure 3. The larger microfibrils in the MFC coated film lowered its transmittance to 79−84%. For the other CN coatings, no significant decrease in the total luminesce transmittance compared to the transmittance of the uncoated plastic film was observed.

The transmittance haze, i.e., the percentage of the scattered light going through a film, was below 7% for all the coatings produced with chemically treated nanocellulose (CNF_L, CNF_M, and CNCs). The haze of the latex coating (LTX) was slightly higher, probably due to light scattering from the coating and its surface roughness. However, optical haze was decreased by coating with the chemically treated nanocelluloses due to their surface smoothening effect. The large microfibrils in the MFC coating increased the light scattering considerably, leading to 71% haze at the wavelength of 400 nm. All the films produced from chemically treated nanocelluloses showed promising optical properties for applications requiring transparency and clarity, e.g., live-cell imaging. The high haze of the MFC film reduces the imaging resolution through them. In contrast, the CNC coating had the lowest haze due to small nanometre-scale particles that do not scatter light.

Wettability and Hydrophilicity. CN coatings are hydrophilic and swell when exposed to liquids, resulting in time-dependent wettability. The initial contact angles decreased 14−29% from their initial values after 5 s (Figure 4). MFC
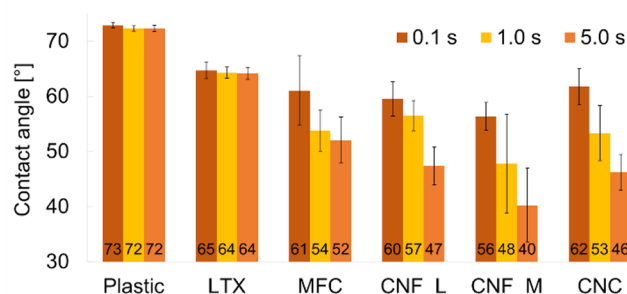

Figure 4. Wetting of the plastic and coatings over 5 s contact times on dry films.

coatings had a higher contact angle compared to TEMPO-treated CNFs and CNCs, which may originate from the lower surface charge of the fibrils. MFC has rougher surface as well which is known to affect surface wetting by decreasing the contact for rougher materials when surface is wetting <90 °C according the Wenzel model. The latex coating and the plastic film had stable contact angles over the inspection period of 5 s. In TEMPO-treated samples nanocellulose absorb water, hence decreasing volume of the drop over longer inspection periods.

Compression Modulus. CN absorbs water and forms hydrogels through its hydrophilic groups, nanoscale size, and entanglement of the fibrils. Water uptake capacity of the CNs is linked to the surface charge of the fibrils and the multivalent-ion concentrations in water-based solutions.[33] Here, we studied gelling of the thin CN coatings bound to a latex coating in three liquids at 37 °C: cell culture medium (DMEM), PBS, and deionized water. The compression elastic moduli of the gelled coatings were characterized with colloidal probe microscopy.

MFC coating was the stiffest of the CN coatings having a Young's modulus in the range 150−350 kPa (Figure 5). Some
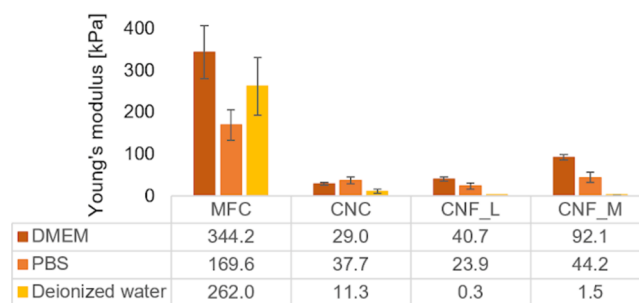

	MFC	CNC	CNF_L	CNF_M
DMEM	344.2	29.0	40.7	92.1
PBS	169.6	37.7	23.9	44.2
Deionized water	262.0	11.3	0.3	1.5

Figure 5. Young's modulus of MFC and cellulose nanomaterial hydrogels films at 37 °C in cell culture media (DMEM), phosphate buffer solution (PBS), and deionized water.

of the measurement points were above the measurement range of the used colloidal probe. Due to the large variability in the fibril size at the coating surface, the compression modulus also had significant variations. The three chemically modified CNs formed softer hydrogels in all three liquids. Calcium, magnesium, and iron ions in DMEM led to ionic-cross-linking of both CNF_L and CNF_M, thereby increasing their

compression moduli to 40.7 and 92.1 kPa, respectively, when compared to the PBS and deionized water. The gel strength is lower for both CNFs in PBS and further in deionized water compared to DMEM due to a deficiency of di- and multivalent ions in PBS and absence of ions in deionized water. The CNF_M has more charged groups than CNF_L, which increases the number of interfibrillar interactions and leads to a stronger hydrogel. Compared to the previous study, the measured compression modulus values are higher.[33] The reason may be in drying at elevated temperatures which can lead to some degrees of hornification, i.e., decreased interfibrillar space and irreversible attractive interactions between the fibrils.[45] Due to the CNC rigid structure and thin coating layer, the measured Young's modulus value seemed lower than expected, and it could possibly originate from the films detachment from the latex layer.

The decrease in compression modulus, i.e., gel strength, when replacing DMEM with PBS, may have adverse effects in cell studies due to the use of PBS as washing liquid in cell fixation and staining protocols. This decrease in gel strength could be reduced by using PBS with added calcium and magnesium salts. Cells are typically sensitive to hydrogel's mechanical and structural changes.[46] Ionic cross-linking could be used as a method to adjust the hydrogel strength.

Cell Culture of Fibroblasts on Cellulose Nanomaterial Coatings. In general, CNs are considered as noncytotoxic materials. However, depending on the added chemicals and chemical modifications, some degree of cytotoxicity has been reported, for instance, with antimicrobial component cetyltrimethylammonium bromide (CTAB).[47] In the current study, the viability of HDFs on the various CN coatings was investigated using four cell seeding densities: 0, 6000, 13,000, and 19,000 cells/cm^2. As a reference, we used a latex coating (LTX) that has been shown to support similar cell growth as glass coverslips.[41] Fluorescence emission images acquired with a gel scanner shown in Figure 6 were used to quantify the cell viability with Calcein-AM staining. Replicates of three of these measurements for each coating type and incubation time (24, 72 h) were used to calculate mean fluorescence intensities s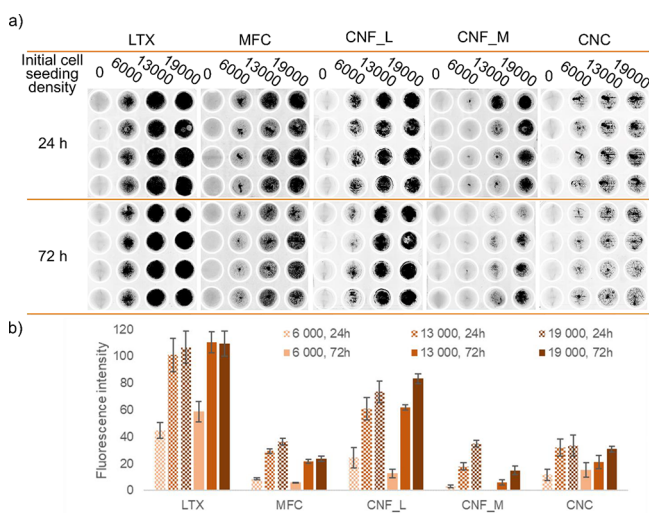hown in Figure 6b. Cell morphologies shown in Figure 7 were studied using fluorescence microscopy to verify the gel scanner results.
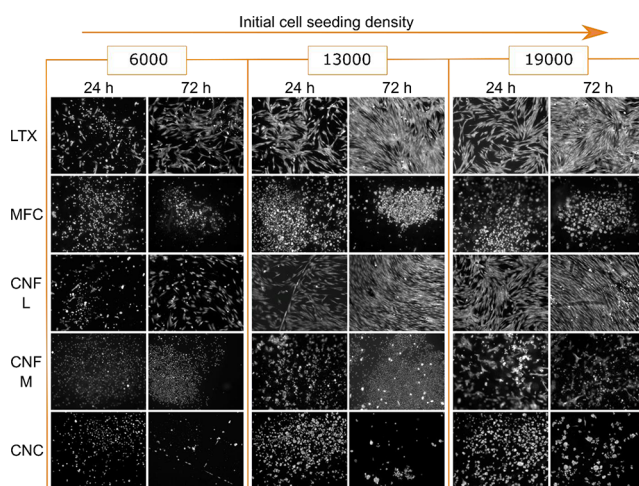

Figure 7. Summary of Calcein-AM stained HDF cell images from the gel scanner samples after 24 and 72 h.

The number of viable cells increased, reflected as an increase in fluorescence intensity, with the increasing cell seeding densities, as expected. On LTX and CNF_L coatings, HDFs achieved confluency at 13,000 cells/cm^2 cell seeding density. Therefore, a similar level of fluorescence intensity should be expected at 13,000 and 19,000 cells/cm^2 cell seeding density on LTX and CNF_L. Instead, CNF_L showed significantly lower intensities after 24 and 72 h compared to LTX. Therefore, it seems that the gel scanner underestimates the number of viable cells in CNF_L and possibly for other CNs. The underestimation may originate from intrinsic fluorescence of the CNs.

In the fluorescence images, LTX and CNF_L coatings show HDFs attached and spread on the surface and the increase in number of cells from 24 to 72 h of incubation. This increase is not visible in the fluorescence intensities (Figure 6). The low surface charged TEMPO-treated CNF_L had the highest fluorescence intensity and the greatest number of cells in the fluorescence image (Figure 7) of the CN coatings, indicating the highest cell viability. CNF_M having a higher total surface charge of 1.5 mmol/g showed visibly reduced cell viability compared to CNF_L, which has been reported previously with other cell lines.[30,48]

Three other CN coatings, MFC, CNF_M, and CNCs, had fewer attached cells after both time points (24, 72 h) than CNF_L, indicating a lower cell adherence on these surface. Furthermore, the decrease in attached cells from 24 to 72 h of incubation shown as a reduction in fluorescence intensity as well as in the number of cells in the images indicates higher cell death rate than proliferation.

On the MFC and CNC coatings, the HDFs were mostly round, implying low adhesion and orientation. Oriented cells on CNC coatings were observed within the cracks of the coatings confirming its noncytotoxicity, but indicating low adherence of HDFs on the sulfated CNC surface, similarly as on MFC. In previous studies, CNCs have supported cell growth in composite materials where cells adhere to the other component and CNCs are used either as a strengthening agent[49,50] or as an aligned sub-monolayer prepared by spin coating to direct cell (myoblast) growth.[25] Similarly to CNCs,

Figure 6. HDF viabilities stained with calcein-AM and measured fluorescence intensities per several cells seeded and after 24 and 72 h. Error bars illustrate the standard deviation in the measurements.

MFC requires either functionalization such as low TEMPO oxidation to introduce carboxyl groups or other chemicals for HDFs to adhere. However, it should be noted that surface roughness and stiffness of biomaterials play a crucial role in cell adhesion as well.

Fibroblast Adhesion to Cellulose Nanomaterial Coatings. Cell adhesion to a surface in vitro comprises three different stages.[51,52] The initial attachment includes the adherence of the rounded cell body to the surface (phase I: sedimentation). Then, cells proceed to flatten and spread onto the surface, thereby increasing the contact area (phase II: cell attachment). At last, cells spread fully onto the surface by reorganizing and distributing the actin skeleton to increase adhesion strength (phase III: cell spreading and stable adhesion). The formation of focal adhesion sites is the main factor involved in the last stage. Vinculin is a protein that is localized in focal adhesion sites when active and within the cytoplasm when inactive. Therefore, cell adhesion to a biomaterial can also be described through the study of vinculin.[53,54]

Figure 8 shows representative images of HDF adhesion to the plant-based CN coatings after 1 day of cell culture. The
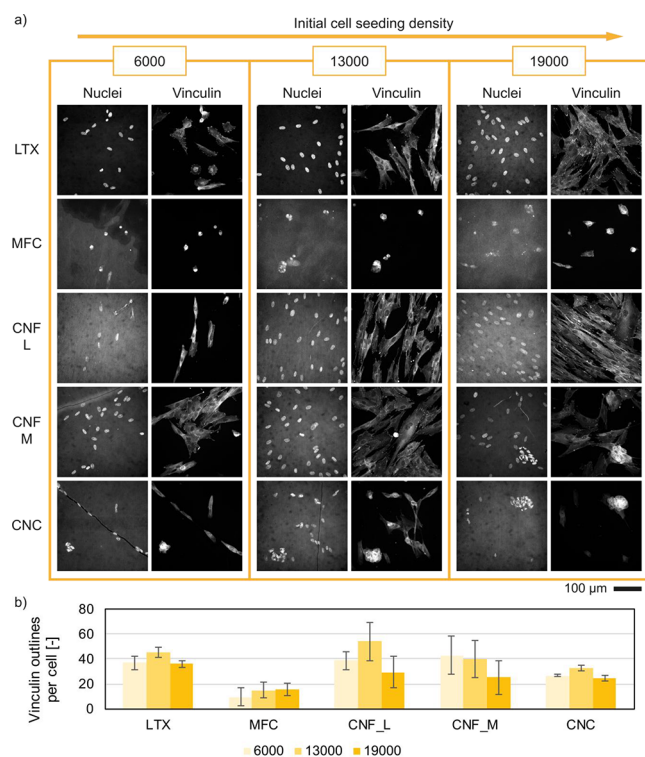

Figure 8. Summary of immunofluorescence staining after 1 day of cell culture on plant-based CN coatings. (a) Representative images of fibroblast adhesion to LTX, MFC, CNF_L, CNF_M, and CNC. The images include nuclear and vinculin staining at the cell seeding densities 6000, 13,000, and 19,000. Additional stainings, such as vimentin and actin, are included in Supporting Information Figure S1. (B) Quantification of vinculin outlines per cell for each coating. Data is represented as an average value with a standard error of the mean.

staining and subsequent imaging provided a description of the cellular morphology, adhesion, and organization resulting from the initial biomaterial−cell interactions. This discussion is focused on the nuclear and vinculin staining, but representative images of vimentin and actin staining can be found in

Supporting Information Figure S1. Images obtained from nuclear staining showed background fluorescence from the coatings.

Morphologically, LTX and CNF_L showed cell adhesion and spreading that significantly improved with increased cell seeding density, which reflects the importance of optimizing cell seeding density for different biomaterials. The behavior was similar for CNF_M, yet the samples had fewer cells, and there was an inconsistent attachment of fibroblasts compared to the Calcein-AM staining. There were also cracks in the films, and in such cases fibroblasts attached nearby. Sometimes, such as in the case of 19,000 cells/cm^2 seeding density in CNF_M, fibroblasts agglomerated into clumps where the nuclei appeared smaller and deformed. The agglomerations were localized and not widespread throughout the samples of CNF_M. In comparison, on CNC coatings, fibroblasts attached and stretched slightly only in the vicinity of the cracks in the film while forming clumps on the rest of the coating. The limited stretching suggests that the cells were arrested before the flattening of phase II of attachment. Lastly, MFC had very few fibroblasts present on the samples. There was no flattening or spreading of the cells, suggesting that the cells were arrested in phase I of attachment, or the adhesion was so weak that they were removed during the staining steps.

In terms of vinculin, the samples with focal adhesion sites were those with fully stretched cells, which was the case for LTX, CNF_L, and CNF_M. Figure 8b shows the quantification of the vinculin outlines per cell in each sample. Cells growing on CNCs and MFC showed mostly cytosolic vinculin and therefore did not count as focal adhesion sites. The lack of focal adhesion sites results in the observed defective cell adhesion. Overall, all samples, with the exception of CNF_L, showed no signs of polarity after cell adhesion. In contrast, fibroblasts on CNF_L seemed to align mainly in one direction. The reason for HDFs alignment on CNF_L requires further investigation.

Inconsistencies between the immunofluorescence staining and the observations with Calcein-AM are probably due to the defects in the coating or cells detaching during staining steps. In cases where the coated film breaks, the cells can potentially grow on top of the latex layer that is placed underneath. The latex undercoat might encourage cell attachment along cracks in the films. However, since the cells are not aligned in the latex coated sample, the alignment observed in the cracks may be guided by the morphological features of the breakage.

■ CONCLUSIONS

Here, we show that once-dried CN coatings absorbed water-based solutions to create soft, transparent hydrogels with low haze and having a compression modulus between 30 and 90 kPa for chemically modified CNs, CNC, CNF_L, and CNF_M. With these optical properties, the thin CN coatings can be used to do live-cell imaging. The Young's modulus and morphology of the films are significantly closer to the characteristics of soft tissues, endothelial, muscle, and cartilage, than to traditional plastic plates, creating a more natural mechanical environment for soft tissues.

We show that, through TEMPO-treatment, anionic hydrogels react to the ion concentration changes, which should be taken into account when cells are grown on the hydrogels and solutions are changed. From cell viability and adhesion data, the CNF_L was the most promising CN type when adhesion is desired. CNF_L allowed cells to adhere to and orient locally

on the coating without any additives, such as fibronectin coatings used to improve anchorage-dependent cell adhesion on CN surfaces. HDFs require chemically compatible CNs to adhere, and for this purpose the carboxylated CNFs with moderate charge and elongated morphology seems to be the most suitable option. In the future, the improved cell adhesion and viability on CNF_L with 1.14 mmol/g total surface charge compared to MFC and CNF_M (1.5 mmol/g) should be further investigated to clarify which surface property from surface charge, crystallinity, fibril size, and topography or changes in hemicellulose residues play the most significant role in the changes in cell adhesion to various cellulose nanomaterials. The other CN coatings here could be used in cell patterning as a nonadherent surface for HDFs. MFC is an exciting material to produce hydrogel wound dressings because of its capacity to absorb water and larger entangled fibrils that make it more robust than CNFs and CNC based films and because of the low adhesion of HDFs on its surface. Similarly, CNC based coatings having low HDF adhesion on their surface have potential applications in biomedical applications as an inert biomaterial.

■ ASSOCIATED CONTENT

Ⓢ Supporting Information

The Supporting Information is available free of charge at https://pubs.acs.org/doi/10.1021/acs.biomac.0c00107.

> Extended methods and results from cellulose nanomaterial production and characterization; extended methods and results from immunofluorescence staining for fibroblast adhesion studies (PDF)

■ AUTHOR INFORMATION

Corresponding Author

Martti Toivakka − *Laboratory of Natural Materials Technology, Åbo Akademi University, 20540 Turku, Finland;* Email: martti.toivakka@abo.fi

Authors

Ruut Kummala − *Laboratory of Natural Materials Technology, Åbo Akademi University, 20540 Turku, Finland;* ⓞ orcid.org/0000-0001-7586-9331

Diosángeles Soto Véliz − *Laboratory of Natural Materials Technology, Åbo Akademi University, 20540 Turku, Finland*

Zhiqiang Fang − *State Key Laboratory of Pulp and Paper Engineering, South China University of Technology, Guangzhou 510640, Guangdong, People's Republic of China;* ⓞ orcid.org/0000-0002-0844-7507

Wenyang Xu − *Laboratory of Natural Materials Technology, Åbo Akademi University, 20540 Turku, Finland*

Tiffany Abitbol − *RISE, Research Institute of Sweden, 11428 Stockholm, Sweden*

Chunlin Xu − *Laboratory of Natural Materials Technology, Åbo Akademi University, 20540 Turku, Finland*

Complete contact information is available at:
https://pubs.acs.org/10.1021/acs.biomac.0c00107

Notes

The authors declare no competing financial interest.

■ ACKNOWLEDGMENTS

■ REFERENCES

(1) De France, K. J.; Hoare, T.; Cranston, E. D. Review of Hydrogels and Aerogels Containing Nanocellulose. *Chem. Mater.* **2017**, *29*, 4609−4631.

(2) Halib, N.; Perrone, F.; Cemazar, M.; Dapas, B.; Farra, R.; Abrami, M.; Chiarappa, G.; Forte, G.; Zanconati, F.; Pozzato, G.; Murena, L.; Fiotti, N.; Lapasin, R.; Cansolino, L.; Grassi, G.; Grassi, M. Potential Applications of Nanocellulose-Containing Materials in the Biomedical Field. *Materials* **2017**, *10*, 977.

(3) Ling, S.; Chen, W.; Fan, Y.; Zheng, K.; Jin, K.; Yu, H.; Buehler, M. J.; Kaplan, D. L. Biopolymer nanofibrils: Structure, modeling, preparation, and applications. *Prog. Polym. Sci.* **2018**, *85*, 1−56.

(4) Portela, R.; Leal, C. R.; Almeida, P. L.; Sobral, R. G. Bacterial cellulose: a versatile biopolymer for wound dressing applications. *Microb. Biotechnol.* **2019**, *12*, 586−610.

(5) Klemm, D.; Kramer, F.; Moritz, S.; Lindström, T.; Ankerfors, M.; Gray, D.; Dorris, A. Nanocelluloses: A New Family of Nature-Based Materials. *Angew. Chem., Int. Ed.* **2011**, *50*, 5438−5466.

(6) Moon, R. J.; Martini, A.; Nairn, J.; Simonsen, J.; Youngblood, J. Cellulose nanomaterials review: structure, properties and nanocomposites. *Chem. Soc. Rev.* **2011**, *40*, 3941−3994.

(7) Basu, A.; Lindh, J.; Ålander, E.; Strømme, M.; Ferraz, N. On the use of ion-crosslinked nanocellulose hydrogels for wound healing solutions: Physicochemical properties and application-oriented biocompatibility studies. *Carbohydr. Polym.* **2017**, *174*, 299−308.

(8) Hakkarainen, T.; Koivuniemi, R.; Kosonen, M.; Escobedo-Lucea, C.; Sanz-Garcia, A.; Vuola, J.; Valtonen, J.; Tammela, P.; Mäkitie, A.; Luukko, K.; Yliperttula, M.; Kavola, H. Nanofibrillar cellulose wound dressing in skin graft donor site treatment. *J. Controlled Release* **2016**, *244*, 292−301.

(9) Liu, Y.; Sui, Y.; Liu, C.; Liu, C.; Wu, M.; Li, B.; Li, Y. A physically crosslinked polydopamine/nanocellulose hydrogel as potential versatile vehicles for drug delivery and wound healing. *Carbohydr. Polym.* **2018**, *188*, 27−36.

(10) Liu, J.; Chinga-Carrasco, G.; Cheng, F.; Xu, W.; Willför, S.; Syverud, K.; Xu, C. Hemicellulose-reinforced nanocellulose hydrogels for wound healing application. *Cellulose* **2016**, *23*, 3129−3143.

(11) Krontiras, P.; Gatenholm, P.; Hagg, D. A. Adipogenic differentiation of stem cells in three-dimensional porous bacterial nanocellulose scaffolds. *J. Biomed. Mater. Res., Part B* **2015**, *103*, 195−203.

(12) Lu, T.; Li, Q.; Chen, W.; Yu, H. Composite aerogels based on dialdehyde nanocellulose and collagen for potential applications as wound dressing and tissue engineering scaffold. *Compos. Sci. Technol.* **2014**, *94*, 132−138.

(13) Markstedt, K.; Mantas, A.; Tournier, I.; Avila, H. M.; Hagg, D.; Gatenholm, P. 3D Bioprinting Human Chondrocytes with Nanocellulose-Alginate Bioink for Cartilage Tissue Engineering Applications. *Biomacromolecules* **2015**, *16*, 1489−1496.

(14) Dugan, J. M.; Gough, J. E.; Eichhorn, S. J. Bacterial cellulose scaffolds and cellulose nanowhiskers for tissue engineering. *Nanomedicine* **2013**, *8*, 287−298.

(15) Torgbo, S.; Sukyai, P. Bacterial cellulose-based scaffold materials for bone tissue engineering. *Appl. Mater. Today* **2018**, *11*, 34−49.

(16) Abitbol, T.; Rivkin, A.; Cao, Y.; Nevo, Y.; Abraham, E.; Ben-Shalom, T.; Lapidot, S.; Shoseyov, O. Nanocellulose, a tiny fiber with huge applications. *Curr. Opin. Biotechnol.* **2016**, *39*, 76−88.

(17) Klemm, D.; Cranston, E. D.; Fischer, D.; Gama, M.; Kedzior, S. A.; Kralisch, D.; Kramer, F.; Kondo, T.; Lindström, T.; Nietzsche, S.; Petzold-Welcke, K.; Rauchfuß, F. Nanocellulose as a natural source for groundbreaking applications in materials science: Today's state. *Mater. Today* **2018**, *21*, 720−748.

(18) Nordli, H. R.; Chinga-Carrasco, G.; Rokstad, A. M.; Pukstad, B. Producing ultrapure wood cellulose nanofibrils and evaluating the cytotoxicity using human skin cells. *Carbohydr. Polym.* **2016**, *150*, 65−73.

(19) Imlimthan, S.; Otaru, S.; Keinänen, O.; Correia, A.; Lintinen, K.; Santos, H.; Airaksinen, A. J.; Kostiainen, M. A.; Sarparanta, M. Radiolabeled Molecular Imaging Probes for the In Vivo Evaluation of Cellulose Nanocrystals for Biomedical Applications. *Biomacromolecules* **2019**, *20*, 674−683.

(20) Hanif, Z.; Ahmed, F. R.; Shin, S. W.; Kim, Y.; Um, S. H. Size- and dose-dependent toxicity of cellulose nanocrystals (CNC) on human fibroblasts and colon adenocarcinoma. *Colloids Surf., B* **2014**, *119*, 162−165.

(21) Mahmoud, K. A.; Mena, J. A.; Male, K. B.; Hrapovic, S.; Kamen, A.; Luong, J. H. T. Effect of Surface Charge on the Cellular Uptake and Cytotoxicity of Fluorescent Labeled Cellulose Nanocrystals. *ACS Appl. Mater. Interfaces* **2010**, *2*, 2924−2932.

(22) Dong, S.; Cho, H. J.; Lee, Y. W.; Roman, M. Synthesis and Cellular Uptake of Folic Acid-Conjugated Cellulose Nanocrystals for Cancer Targeting. *Biomacromolecules* **2014**, *15*, 1560−1567.

(23) Dong, S.; Hirani, A. A.; Colacino, K. R.; Lee, Y. W.; Roman, M. Cytotoxicity and cellular uptake of cellulose nanocrystals. *Nano LIFE* **2012**, *2*, 1241006.

(24) Metwally, S.; Stachewicz, U. Surface potential and charges impact on cell responses on biomaterials interfaces for medical applications. *Mater. Sci. Eng., C* **2019**, *104*, 109883.

(25) Dugan, J. M.; Collins, R. F.; Gough, J. E.; Eichhorn, S. J. Oriented surfaces of adsorbed cellulose nanowhiskers promote skeletal muscle myogenesis. *Acta Biomater.* **2013**, *9*, 4707−4715.

(26) Smyth, M.; M'Bengue, M.; Terrien, M.; Picart, C.; Bras, J.; Foster, E. J. The effect of hydration on the material and mechanical properties of cellulose nanocrystal-alginate composites. *Carbohydr. Polym.* **2018**, *179*, 186−195.

(27) Vielreicher, M.; Kralisch, D.; Völkl, S.; Sternal, F.; Arkudas, A.; Friedrich, O. Bacterial nanocellulose stimulates mesenchymal stem cell expansion and formation of stable collagen-I networks as a novel biomaterial in tissue engineering. *Sci. Rep.* **2018**, *8*, 9401.

(28) Skogberg, A.; Mäki, A.; Mettänen, M.; Lahtinen, P.; Kallio, P. Cellulose Nanofiber Alignment Using Evaporation-Induced Droplet-Casting, and Cell Alignment on Aligned Nanocellulose Surfaces. *Biomacromolecules* **2017**, *18*, 3936−3953.

(29) Xu, W.; Wang, X.; Sandler, N.; Willför, S.; Xu, C. Three-Dimensional Printing of Wood-Derived Biopolymers: A Review Focused on Biomedical Applications. *ACS Sustainable Chem. Eng.* **2018**, *6*, 5663−5680.

(30) Liu, J.; Cheng, F.; Grenman, H.; Spoljaric, S.; Seppala, J.; Eriksson, J. E.; Willfor, S.; Xu, C. Development of nanocellulose scaffolds with tunable structures to support 3D cell culture. *Carbohydr. Polym.* **2016**, *148*, 259−271.

(31) Caliari, S. R.; Burdick, J. A. A practical guide to hydrogels for cell culture. *Nat. Methods* **2016**, *13*, 405−414.

(32) Buxboim, A.; Rajagopal, K.; Brown, A. E. X.; Discher, D. E. How deeply cells feel: methods for thin gels. *J. Phys.: Condens. Matter* **2010**, *22*, 194116.

(33) Kummala, R.; Xu, W.; Xu, C.; Toivakka, M. Stiffness and swelling characteristics of nanocellulose films in cell culture media. *Cellulose* **2018**, *25*, 4969−4978.

(34) Basu, A.; Heitz, K.; Strømme, M.; Welch, K.; Ferraz, N. Ion-crosslinked wood-derived nanocellulose hydrogels with tunable antibacterial properties: Candidate materials for advanced wound care applications. *Carbohydr. Polym.* **2018**, *181*, 345−350.

(35) Zander, N. E.; Dong, H.; Steele, J.; Grant, J. T. Metal Cation Cross-Linked Nanocellulose Hydrogels as Tissue Engineering Substrates. *ACS Appl. Mater. Interfaces* **2014**, *6*, 18502−18510.

(36) Kumar, V.; Nazari, B.; Bousfield, D.; Martti, T. Rheology of microfibrillated cellulose suspensions in pressure-driven flow. *Appl. Rheol.* **2016**, *26*, 1−11.

(37) Schneider, C. A.; Rasband, W. S.; Eliceiri, K. W. NIH Image to ImageJ: 25 years of image analysis. *Nat. Methods* **2012**, *9*, 671−675.

(38) Soto Veliz, D.; Zhang, H.; Toivakka, M. Stacking up: a new approach for cell culture studies. *Biomater. Sci.* **2019**, *7*, 3249−3257.

(39) Mayet, N.; Choonara, Y. E.; Kumar, P.; Tomar, L. K.; Tyagi, C.; Toit, L. C. D.; Pillay, V. A Comprehensive Review of Advanced Biopolymeric Wound Healing Systems. *J. Pharm. Sci.* **2014**, *103*, 2211−2230.

(40) Coulomb, B.; Lebreton, C.; Dubertret, L. Influence of Human Dermal Fibroblasts on Epidermalization. *J. Invest. Dermatol.* **1989**, *92*, 122−125.

(41) Rosqvist, E.; Niemelä, E.; Venu, A. P.; Kummala, R.; Ihalainen, P.; Toivakka, M.; Eriksson, J. E.; Peltonen, J. Human dermal fibroblast proliferation controlled by surface roughness of two-component nanostructured latex polymer coatings. *Colloids Surf., B* **2019**, *174*, 136−144.

(42) Rueden, C. T.; Schindelin, J.; Hiner, M. C.; DeZonia, B. E.; Walter, A. E.; Arena, E. T.; Eliceiri, K. W. ImageJ2: ImageJ for the next generation of scientific image data. *BMC Bioinf.* **2017**, *18*, 529.

(43) Schindelin, J.; Arganda-Carreras, I.; Frise, E.; Kaynig, V.; Longair, M.; Pietzsch, T.; Preibisch, S.; Rueden, C.; Saalfeld, S.; Schmid, B.; Tinevez, J.; White, D. J.; Hartenstein, V.; Eliceiri, K.; Tomancak, P.; Cardona, A. Fiji: an open-source platform for biological-image analysis. *Nat. Methods* **2012**, *9*, 676−682.

(44) McQuin, C.; Goodman, A.; Chernyshev, V.; Kamentsky, L.; Cimini, B. A.; Karhohs, K. W.; Doan, M.; Ding, L.; Rafelski, S. M.; Thirstrup, D.; Wiegraebe, W.; Singh, S.; Becker, T.; Caicedo, J. C.; Carpenter, A. E. CellProfiler 3.0: Next-generation image processing for biology. *PLoS Biol.* **2018**, *16*, No. e2005970.

(45) Fernandes Diniz, J. M. B.; Gil, M. H.; Castro, J. A. A. M. Hornification—its origin and interpretation in wood pulps. *Wood Sci. Technol.* **2004**, *37*, 489−494.

(46) Caliari, S. R.; Burdick, J. A. A practical guide to hydrogels for cell culture. *Nat. Methods* **2016**, *13*, 405−414.

(47) Alexandrescu, L.; Syverud, K.; Gatti, A.; Chinga-Carrasco, G. Cytotoxicity tests of cellulose nanofibril-based structures. *Cellulose* **2013**, *20*, 1765−1775.

(48) Novotna, K.; Havelka, P.; Sopuch, T.; Kolarova, K.; Vosmanska, V.; Lisa, V.; Svorcik, V.; Bacakova, L. Cellulose-based materials as scaffolds for tissue engineering. *Cellulose* **2013**, *20*, 2263−2278.

(49) Domingues, R. M. A.; Silva, M.; Gershovich, P.; Betta, S.; Babo, P.; Caridade, S. G.; Mano, J. F.; Motta, A.; Reis, R. L.; Gomes, M. E. Development of Injectable Hyaluronic Acid/Cellulose Nanocrystals Bionanocomposite Hydrogels for Tissue Engineering Applications. *Bioconjugate Chem.* **2015**, *26*, 1571−1581.

(50) Yang, X.; Bakaic, E.; Hoare, T.; Cranston, E. D. Injectable Polysaccharide Hydrogels Reinforced with Cellulose Nanocrystals: Morphology, Rheology, Degradation, and Cytotoxicity. *Biomacromolecules* **2013**, *14*, 4447−4455.

(51) Hong, S.; Ergezen, E.; Lec, R.; Barbee, K. A. Real-time analysis of cell−surface adhesive interactions using thickness shear mode resonator. *Biomaterials* **2006**, *27*, 5813−5820.

(52) Khalili, A. A.; Ahmad, M. R. A Review of Cell Adhesion Studies for Biomedical and Biological Applications. *Int. J. Mol. Sci.* **2015**, *16*, 18149−18184.

(53) Chen, H.; Cohen, D. M.; Choudhury, D. M.; Kioka, N.; Craig, S. W. Spatial distribution and functional significance of activated vinculin in living cells. *J. Cell Biol.* **2005**, *169*, 459−470.

(54) Bays, J. L.; DeMali, K. A. Vinculin in cell−cell and cell−matrix adhesions. *Cell. Mol. Life Sci.* **2017**, *74*, 2999−3009.